

# Linking Scars: Topology-based Scar Detection and Graph Modeling of Paleolithic Artifacts in 3D

Florian Linsel<sup>1</sup>, Jan Philipp Bullenkamp<sup>1</sup> & Hubert Mara<sup>1</sup>

<sup>1</sup> Institute of Computer Science, Martin-Luther University of Halle-Wittenberg – Halle, Germany

**Correspondence:** [florian.linsel@informatik.uni-halle.de](mailto:florian.linsel@informatik.uni-halle.de)

## Abstract

Motivated by the concept of combining the archaeological practice of creating lithic artifact drawings with the potential of 3D mesh data, our goal in this project is not only to analyze the shape at the artifact level, but also to enable a more detailed analysis of stone tools at the scar and ridge level. For this purpose, we combine the archaeological interpretation, typically represented in 2D, with its corresponding 3D data. To achieve this goal, we propose a workflow that utilizes 3D datasets as the best means for shape analysis of lithic artifacts, which relies on one of the first open access repositories of 3D scanned lithic tools. In our four-step workflow, we start with a preprocessing in GigaMesh, followed by a scar segmentation using Morse theory-based algorithms, continue with a postprocessing and finally create a graph model-based representation of the lithic artifacts in 3D. This prototypical graph model can already be used to display and evaluate manual or parameterized operational sequences in 3D. The source code and the manually annotated ground truth data are available as open-access publications under a Creative Commons license.

**Keywords:** Scar detection; 3D meshes; Paleolithic; Operational Sequences; Computational Archaeology

1  
2  
3  
4  
5  
6  
7  
8  
9  
10  
11  
12  
13  
14  
15  
16

## Introduction

17

Lithic artifacts display varying shapes and forms due to the differences in raw material quality and knapping techniques utilized during their production. Of particular interest is the knapping process, which allows the study of each production step, since Paleolithic artifacts remain unpolished. These production steps leave convex and concave scars behind that are separated by ridges (Fig 1). In contemporary archaeology, drawings and images of artifacts, often supported by additional details, are the standard approaches to documenting them.

18

19

20

21

22

23

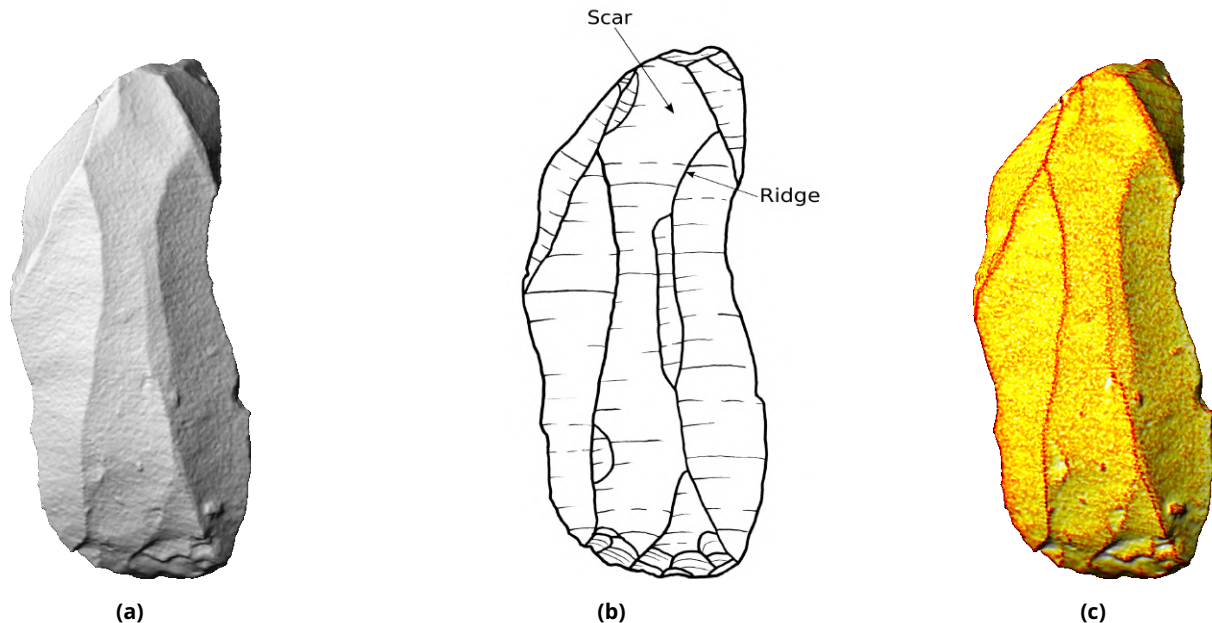


**Figure 1.** Images of artifact *GdF 31*: (a) orthographic projection of the scanned object; (b) drawing of the artifact; (c) MSII-curvature mapped as function value.

One of the pieces of information that can be added to a drawing, is the temporal relation between scars and ridges. In this complex analytical approach, scar-ridge patterns are utilized to establish the sequence of working steps or scars, leading to the analysis of an *operational sequence* (abbr. OS, fr. chaîne opératoire) (Pastoors et al., 2015; Richter, 1997; Richter, 2004). Because identifying scars and ridges can be time-consuming, it is still easier to automate comparisons of the overall artifact shape.

24

26

27

28

29

Since the introduction of Geometric Morphometrics methods in 2D, the analysis of outlines has become more common. Currently, standardized drawings can even be analyzed at the level of individual scars (Gellis et al., 2022). However, the analysis of 3D models in archaeology is still in its early stages. Some approaches involve the use of manually placed landmarks to extract features from the surface of artifacts, such as the overall shape (Herzlinger and Grosman, 2018) or the angle of the cutting edges (Weiss, 2020).

30

31

32

33

34

35

36

Similar to drawings, users of lithic artifact annotations mark specific surface features on the 3D model. In the case of a drawing, the illustrator recognizes and draws the ridges, while in the case of annotation, the annotator does the same, but annotates the scars. In both cases, scars and ridges are directly or indirectly determined. To our knowledge, only a few annotators are currently available, such as those for cuneiform tablets (Homburg et al., 2022) and for lithic artifacts (Pop, 2019).

37

38

39

40

41

42

Besides the manual annotation of scars and ridges, they can also be (semi-) automatically segmented. 3D segmentation is a well known practice to separate 3D models to smaller coherent areas. Segmentation is up to today an under-investigated practice in paleolithic archaeology. Only a handful of approaches are using

43

44

45

3D models to detect scars or ridges. While some approaches use 3D models to extract a 2D rendering in a drawing-like fashion (Barone et al., 2018), other approaches implemented algorithms to automatically segment them on the meshes. Pulla et al. (2001) proposed one of the first methods utilizing a watershed model and varied curvature measurements. The most well-known work in this field is Richardson et al. (2014). In this study, the authors utilized a principal curvature-based geodesic clustering to oversegment lithic artifacts. They merged weak borders and optimized the graph-cut to obtain the scar segmentation. Subsequently, they constructed an adjacency graph model.

The motivation of our research is to visualize labeled 3D models as 3D representations of OS's. Thus, it is necessary to analyze scar-ridge patterns for two objectives: firstly, to segment scars and secondly, to analyze OS's of lithic artifacts, as strongly suggested during our presentation's discussion. Therefore, we introduce a Morse theory-based segmentation approach and an adjacency graph model of neighbouring scars to simplify the 3D model. By considering the relative properties of the scar nodes, we have developed a definition of link direction based on parameters. In this study, we show our workflow leading from the annotation, over the segmentation towards a proof of concept for determining the link directions of scar-ridge graph models.

## Archaeological Practice

**Technical Drawings:** For most artifacts, from ceramics, over bronze knives to lithic tools, one of the primary documentation techniques is a technical drawing. The process of depiction is, according to specialist, an essential part of the archaeological education. Each category of artifact has its own tradition of how it should be represented and drawn. In the following, the most common way how Paleolithic stone artifacts are depicted and drawn (Shea, 2013) will be described. Due to the sequential information imprinted on the dorsal side of the artifact, the dorsal side gets depicted preferably while other views are additional. In a general analysis, all flakes and especially blades are orientated with the pointed side upwards (distal part at the top) and the point of impact, the striking platform, at the bottom of the main view. The artifacts are orientated according to their biggest extent in the y-axis. This digitisation standard applies only to two-dimensional depiction of artifacts, but relying on it, modern approaches using 3D models are following its lead.

**Operational Sequences:** To determine the OS's, multiple attributes are defined (Pastoors et al., 2015), which specify the ridge patterns of adjacent scars. One of these conditions of distinguishing the temporal relation between scars is that "a younger scar contours follows the older scar contour and cuts across it". This process leads to an overprinting and reducing of the more central, older scar. In general, a more central scar, which rings true especially for bigger artifacts like handaxes, is older than scars on the edge. Even if bifaces are not the subject of this research, similar considerations should also be applicable for blade and bladelets. Hence, the positional integration of the scar inside of a scar ridge pattern should be considered.

For a better understanding of artifacts, especially for the procedural relationship between the scars, a graph representation is helpful for understanding the scar-ridge connections (Richardson et al., 2014). Graph models in the form of Harris matrices are used to represent the relation between working stages of lithic artifacts (e.g. Pastoors (2000), Pastoors et al. (2015), and Richter (2004)). In this research, they created Harris matrices from working stages not scars. In this line of thought, scars are assigned to working stages, which are considered to be procedural steps of the knapping. The representation of each scar in a Harris matrix is rather uncommon. However, by providing attributes to determine the relation between adjacent scars (Pastoors et al., 2015), a graph model of lithic artifacts is worth exploring. The basic concept was already applied to experimental data in the context of a refitting (Yang et al., 2017), but it was as far as we know, not applied to real archaeological data. The creation of graph models will serve as an important step towards real archaeological data and can give insights into the production patterns.

## Material and Methods

### Dataset

In this study, an open dataset of lithic artifacts from the *Grotta di Fumane* (GdF) site (Falcucci and Peresani, 2022b) was used. GdF is a north-eastern Italian site, which is well-known for one of the earliest cave paintings in Europe as well as layers clearly associated with the Uluzzian. The Uluzzian, a transitional industry, is one of the earliest techno-complexes associated with the AMHs arrival in Europe (Marín-Arroyo et al., 2023). All artifacts from the dataset are attributed to the on this site following Proto-Aurignacian and are either made from blade or bladelet blanks. Many of the blades and bladelets, especially the intermediate slender blades stay unretouched (Falcucci, Conard, et al., 2017).

From the 732 published artifacts, we selected 57 artifacts from the A1-A2 unit, which is dated between 42,000 and 39,250 cal BP. To gain a broader perspective, we included also 5 artifacts from the D3 unit (D3b, D3d and D3d base), which is dated between 40,000 and 37,750 cal BP (Higham et al., 2009; Marín-Arroyo et al., 2023). A total of 62 artifacts were selected according to their varying scar-ridge complexity.

To compensate for the absence of the original artifact, the annotation workflow was created to determine whether ridges and scars are applicable even when the artifact is not available. In order to get a better representation of the scar-ridge patterns than using conventional rendering techniques, the dataset was pre-processed using the 3D *Multi-Scale Integral Invariant* (MSII) filter and selecting the maximum curvature (Mara and Krömker, 2013) (Fig 2). It is recommended to use a dual monitor or widescreen monitor to use MeshLab (Cignoni et al., 2008) and GigaMesh side by side. While examining the ridges in GigaMesh, MeshLab's Z-painting tool is used to color code the different segments of the mesh surfaces. This creates a dataset that closely approximates the *ground truth* (GT). It is worth noting that the annotations may vary when multiple experts are involved given the absence of a deterministic solution.

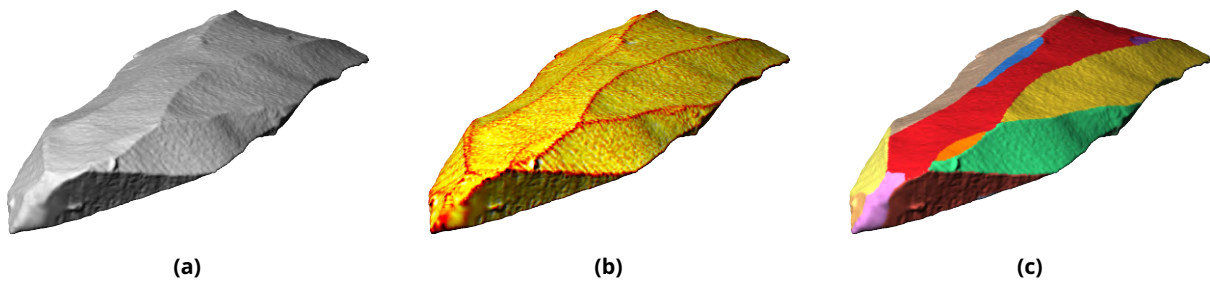


**Figure 2.** Artifacts (*GdF 31*) turned in position to be annotated: (a) original 3D mesh; (b) MSII values (GigaMesh) mapped 3D mesh; (c) with MeshLab color painted 3D mesh

Each manually applied color i.e. graphical annotation represents a labeled connected component. This labeled dataset will serve first, as GT dataset to evaluate the segmentation results and second, to determine the precision of the adjacency graph models. Beside annotated meshes, for the evaluation of the directed graph models, manual OS's were needed. Due to the differing quality of the 3D models, which varies between 40,000 and 400,000 vertices, the relation between scars cannot be determined in some cases, e.g. GdF 710. For the GdF 207, we were able to reconstruct with a high confidence an OS. One additional OS was published in Falcucci, Conard, et al. (2017), from which a directed graph model was generated. The artifact is a multiplatform core (ID: GdF RF.c\_49). It was not part of the initial GdF dataset (Falcucci and Peresani, 2022b) and was added in the later version 2.1.1 (Falcucci and Peresani, 2022a).

## Methods 125

This section presents a four-step workflow for the analysis of lithic artifacts. In the first step, the 3D meshes are preprocessed in the GigaMesh software, then their scars are segmented using Morse theory. The third step is a postprocessing step, and the fourth step is to create an adjacency graph model-based on the annotation. 126  
127  
128  
129

### 1. Preprocessing in GigaMesh (Mara, Krömker, et al., 2010) 130

(a) Orienting, Cleaning and Filling 131

(b) *3D Multi-Scale Integral Invariant* (MSII) Filtering 132

### 2. Scar Segmentation using Morse Theory 133

(a) Morse-Smale Complex 134

(b) Weak and Strong Ridges 135

(c) Oversegmentation (Morse Cells) 136

(d) Merging Morse Cells based on Ridges 137

### 3. Extracting Spatial Properties of Annotated 3D Meshes 138

### 4. Scar-Ridge-Patterns as Graph Models 139

(a) Scar-Ridge Graph as Source for Digital Drawings 140

(b) Directing the Graph Model by Parameter 141

This step by step process will be presented in the following subsections. 142

## Preprocessing in GigaMesh 143

The workflow starts by automatically cleaning and filling the surface of the meshes using the command line tool in GigaMesh. Every 3D mesh by its nature has natural or artificial openings, holes, and gaps on its surface on one side and topological errors due to, e.g., imperfect scan alignment on the other side. Due to the simplicity of lithic artifacts, e.g. no natural and artificial holes, the default setting of the tool can be used. 144  
145  
146  
147  
148

The next step is to orient the artifact using a 3-step procedure: First, calculate the principal orientation based on vertex coordinates and check the mesh for mirroring. Second, a k-means clustering algorithm was utilized to distinguish between the dorsal (front) and ventral (back) sides. Third, the distal (top) and proximal (bottom) orientations are determined by the relationship between the center of mass of the artifact and the location of the centroid of its bounding box (Maier et al., 2023). 149  
150  
151  
152  
153  
154

Finally, the maximum of the MSII curvature is then calculated as an approximation of the maximum curvature (Mara and Krömker, 2013). 155  
156

## Scar Segmentation using Morse Theory 157

The segmentation method used to detect scars originates from Morse theory, which is a technique from differential topology, that has a discrete counterpart introduced by Forman (2001). To use this discrete Morse theory, a mesh with vertices that have a scalar function assigned to them is required. The scalar function used for scar and ridge detection are the maximum MSII curvature values, since they already visually highlight the ridges. 158  
159  
160  
161  
162  
163

**Morse-Smale Complex:** Following the algorithms described in Robins et al. (2011), discrete Morse theory allows to calculate a combinatorial gradient on the mesh, that leads to the detection of minima, saddle points 164  
165

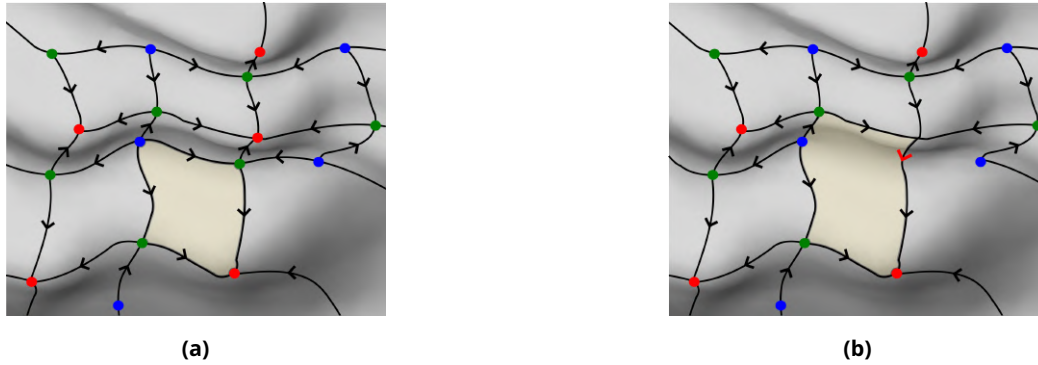


**Figure 3.** (a) MS complex; (b) simplified MS complex

and maxima (also called critical points) on the surface taking into account the underlying scalar function of the vertices. This allows to extract so-called Morse-Smale complexes (MS complexes) by calculating the adjacencies of these extremal points. The adjacency can be retrieved as lines, so-called separatrices, by following the steepest gradient from maxima to saddle points as well as the steepest gradient from saddle points to minima.

The resulting skeleton-like structure on the mesh can be seen in Fig 3 (a), which schematically depicts a hill and dale surface, with the height function as a scalar function for Morse theory. The maxima (blue), saddle points (green) and minima (red) are shown as well as the separatrices (arrows) connecting them. Note that, by definition, there are no separatrices connecting maxima to minima. Such a MS complex on the mesh automatically indicates a segmentation and divides the surface into regions that are enclosed by separatrices, known as Morse cells. One is highlighted in Fig 3 (a) as an illustration.

**Weak and Strong Ridges:** Separatrices represent extremal lines, so they can be used to filter for weak and strong ridges. The mean curvature value of the vertices of a separatrix is used as the importance measure and a double threshold is used to get weak and strong ridges, adding the weak ridges only if they are adjacent to a strong ridge. Fig 4 (a) shows the resulting ridges on an example artifact. The advantage over a thresholding on the whole vertices lies in the nature of separatrices, as they are thin connected lines already and taking the mean curvature value along them allows to bridge short interruptions in the ridges.

**Oversegmentation (Morse Cells):** The next step is getting an oversegmentation of the mesh that aligns with the already detected ridges. Morse theory already provides a natural segmentation, but real datasets contain noise and make this segmentation very fine grained. The skeleton can be simplified by removing small local minima or maxima when their function value distance to the next saddle is below a threshold. A possible step of such a simplification is shown in Fig 3 (b), which leads to enlarged Morse cells. For the segmentation method, Morse cells of a slightly simplified skeleton are taken. This removes noise and ensures that the oversegmentation has cells which are not too small and also keeps the detected ridges in between the Morse cells. Fig 4 (b) shows such an oversegmentation.

**Merging Morse Cells based on Ridges:** Using the oversegmentation and the detected ridges, a weighted adjacency graph can be created using the Morse cells from the oversegmentation. The weights are defined as the percentage of detected ridge points along the boundary between two cells. As a final step, neighboring cells that have no or not enough ridge points detected along their boundary can be iteratively merged. This leads to a final segmentation result (Fig 4 (c)) that ensures that there is a predefined percentage of ridge points between all cells.

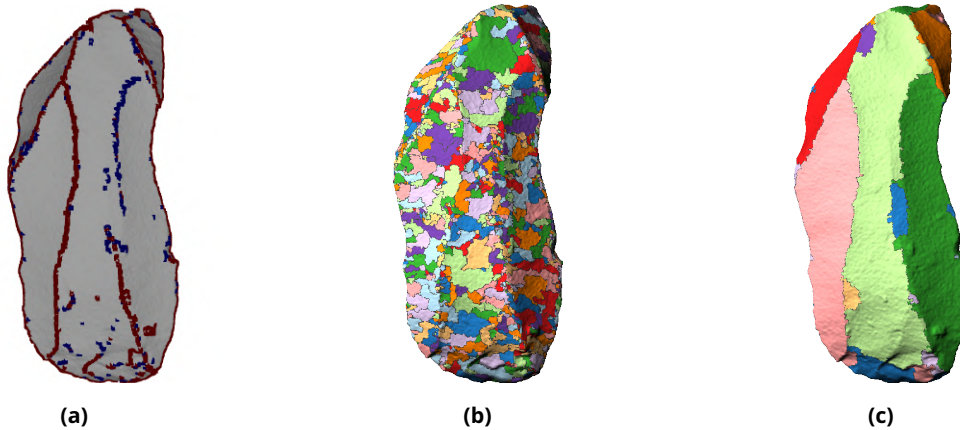


**Figure 4.** (a) Ridges: strong ridges (red), weak ridges (blue); (b) Oversegmentation; (c) Merging (result);

### Extracting Spatial Properties of Annotated 3D Meshes



To demonstrate the process with a final, adjusted segmentation, the ground truth data is used; if done correctly, the ground truth data should be the goal of the segmentation algorithm anyway. Once annotations have been obtained, all colors must be translated into respective labels. Here, due to the high number of scars and the limited number of easily accessible colors in MeshLab, colors can be used repeatedly. Consequently, color values are collected and the data is relabeled to isolate only connected components. Each connected component corresponds to one scar. These connected components are then used to divide the 2D manifold into distinct submeshes.

Each connected component has a contour, which can be represented as a polyline. A contour is a circular line consisting of vertices, where each vertex has neighbors from a different connected component. Additionally, each vertex of a contour has 2 neighbors that belong to the same connected component.

These connected components serve as basis for determining the ridges of an artifact. In fact, the contour set is determined by selecting every contour vertex and every face that contains only contour vertices. In a subsequent step, this set of contours can be divided into segments, each of which represents a ridge. Thus, a ridge can be defined as an area where two or more scars share adjacent contours.

### Scar-Ridge-Patterns as Graph Models

In this chapter, the overall approach for representing the connections of scar-ridge patterns using a graph model gets introduced and analysed to determine the direction of their links. Additionally, the visualization of directed and undirected graph models in 3D will be introduced.

**Scar-Ridge Graph as Source for Digital Drawings:** The scar-ridge pattern serves as a source for digital drawings. From the scar-ridge patterns, an adjacency graph model can be abstracted. In this model, each scar is represented as a node. The existence of an undirected link between two nodes is determined by their neighborhood. Therefore, each ridge can be represented as a link due to the adjacency of the scars. To answer the question of where a scar ends and the ridge begins, it is necessary to differentiate between a scar contour and a ridge segment. This will help to untangle the strong connection between scars and ridges.

While creating the graph model, various properties can be included to specify node or link parameters, such as spatial and non-spatial parameters of scars or ridges. Spatial parameters can include the area of the scar or the mean of a selected parameter, such as the mean MSII curvature values within a scar. In addition to

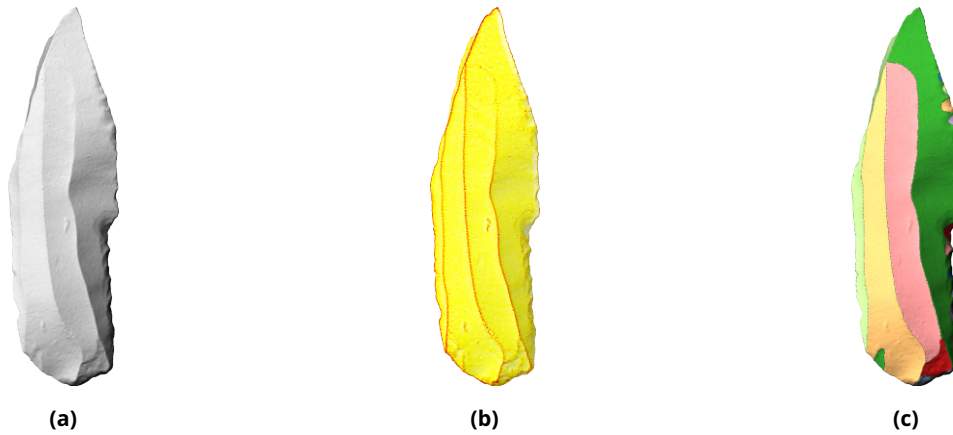


**Figure 5.** Rendered images of artifact *GdF 207*: (a) Solid view; (b) MSII light view (1.0 mm); (c) GT label view

imported scar or ridge parameters, graph parameters describing the relationships between nodes and links can be calculated and used.

In contemporary archaeological practice, the ideal representation of an artifact is a technical drawing that captures the ridges and ripple lines. Having a high-resolution 3D model allows to render alternative images as well as new means of representing a lithic tool assisting in determining the OS. So two renderings were created, one similar to conceptual drawing and one as a graph model depicting the relations (or connections) between surface segments, i.e. scars and ridges.

In the following graph visualization, scars are represented by spheres. The location of the node is determined by the center of mass of each scar. If the node has to be on the surface of the manifold, the closest point to the center of mass can be selected.

In addition to the scar properties, the segmentation of scar contours into ridges is another relevant parameter. The scar contour is an ordered list of vertices that form a circular closed polyline. When performed ideally, ridges can be viewed as the contour segment where two contours share neighboring vertices. Thus, each ridge can be considered as two segments comprised of two contours and due to the right orientation of the faces, these are oppositely oriented. All vertices belonging to the ridge can also be considered as link properties.

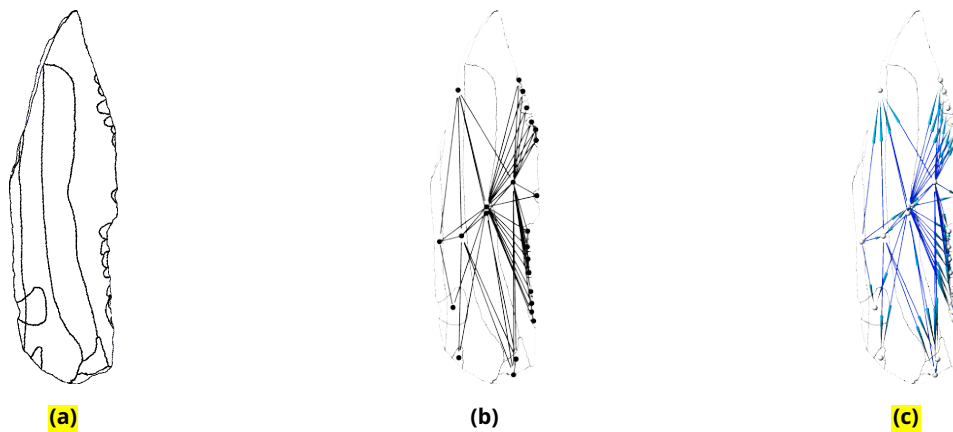


**Figure 6.** *GdF 207* models: (a) 3D ridge model; (b) adjacency graph model and ridge model; (c) directed adjacency graph model (direction = manual)



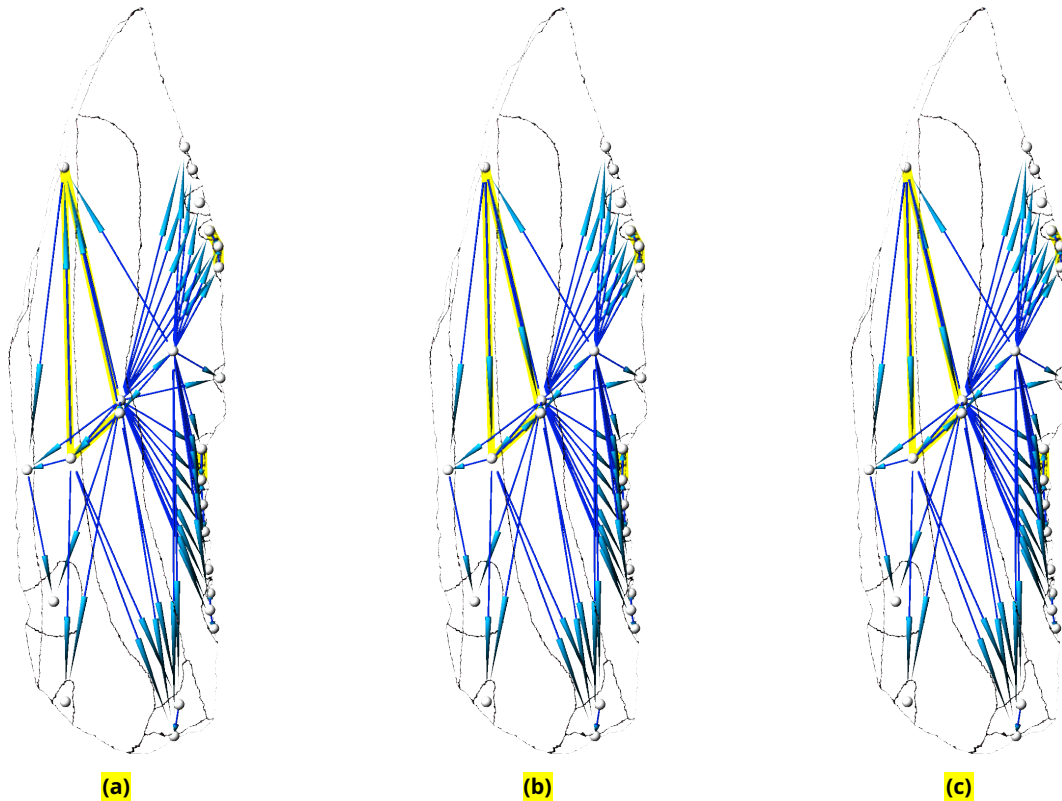


**Figure 7.** Directed 3D graph model of *GdF 207* depicting differences in link orientations (yellow): (a) directed by scar area ("greater"); (b) directed by degree ("greater"); (c) directed by betweenness ("greater")

In this study, we focus on visualizing all contours and therefore filter the mesh for faces consisting of contour vertices only (Fig 6 (a)). In the final visualization of the ridge graph model, everything from the nodes over the ridges to the connections in the form of cylinders (Fig 6 (b)) or arrows (Fig 6 (c)) had to be combined and finally exported.

**Directing the Graph Model by Parameter:** Every undirected graph model possesses properties directly derived from the connectivity of each node and link, such as degree or betweenness centrality. The degree of a node in a graph is the number of nodes that are connected to it by links. Betweenness centrality measures node accessibility. A node with a high betweenness provides insight into the importance of the node in accessing other parts of the graph. A node's betweenness centrality is higher if it needs to be crossed more often to reach other nodes. Conversely, a node on the periphery has a low betweenness centrality.

The procedure for the three parameters is similar. First, an undirected graph model is created. Then the parameter of either the mesh or the graph is extracted and computed. Finally, the difference between two adjacent nodes is estimated. Specifically, the relative difference in area, degree, and betweenness centrality of two adjacent scars are examined to obtain the direction of a link. Due to the exploratory nature of the research, the difference between the nodes was defined as the links direction either from the node with the lower value to one with the higher value ("greater"), or vice versa ("lower") (Fig 7). In this context, indegree describes the number of directed links to a node, outdegree the opposite.

## Results and Evaluation

271

The results presented in this study are divided into two parts: first, the segmentation, where quantitative data is available. Second, creating and visualizing graph models, where a proof of concept is provided.

272

273

### Segmentation Results

274

The described segmentation method was implemented in Python and published in Bullenkamp et al. (2023). The method requires four parameters: persistence for the level of simplification in the oversegmentation, weak and strong ridge thresholds for filtering ridges and a merging parameter for the weighted adjacency graph simplification. Determining these parameters can be laborious. However, the segmentation algorithm is accompanied by a graphical user interface. This allows the user to adjust parameters and obtain visual feedback rather than executing code and importing results into another software for each parameter combination. Furthermore, this article utilizes a pipeline approach to run the segmentation for various parameters and evaluate each combination with the ground truth data (Linsel et al., 2023). Taking the best result for each artifact enables a quantitative evaluation of the segmentation method. For the 62 artifacts with ground truths, the average percentage of correctly labeled vertices is 91.26%, ranging from 81.2% to 97.2%.

275

276

277

278

279

280

281

282

283

284

285

In Fig 8 some representative results are shown, including the best (e) and worst (d) results of the dataset. Artifacts (b), (d), and (h) all have cortex areas, that are supposed to be one label. However, given their rough surface, they have high curvature values that lead to false ridge detection and an oversegmentation of these areas. In Fig 8 (g) there is an artifact that gives a good overall result, but two small scars on the right side are not detected. These scars are too small and the ridge between them and the large scar is too weak. Especially artifacts with clear ridges like Fig 8 (a), (c), (e) and (f) show good results.

286

287

288

289

290

291

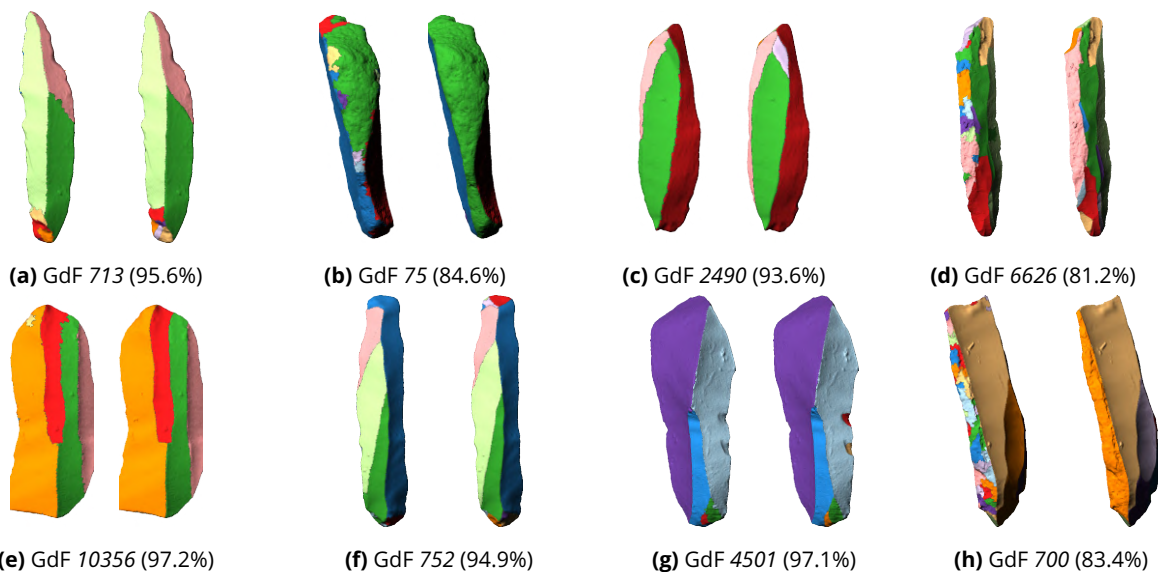


Figure 8. Difference between results (left) and ground truths (right).

### Proof of Concept of Graph Modeling

292

Due to the early stage of this approach, this study will only present prototypical approach of how to use and visualize graph models of lithic artifacts. Digital graph models of lithic artifacts extends the analytical potential of OS's from a manual towards data-driven approaches.

293

294

295

296

In the case of GdF 207, the relationship between the scars is not difficult to follow with a normal OS diagram for an expert, as shown in Fig 9 (a). But as the complexity of the scar pattern increases, the ability to under-

297

298

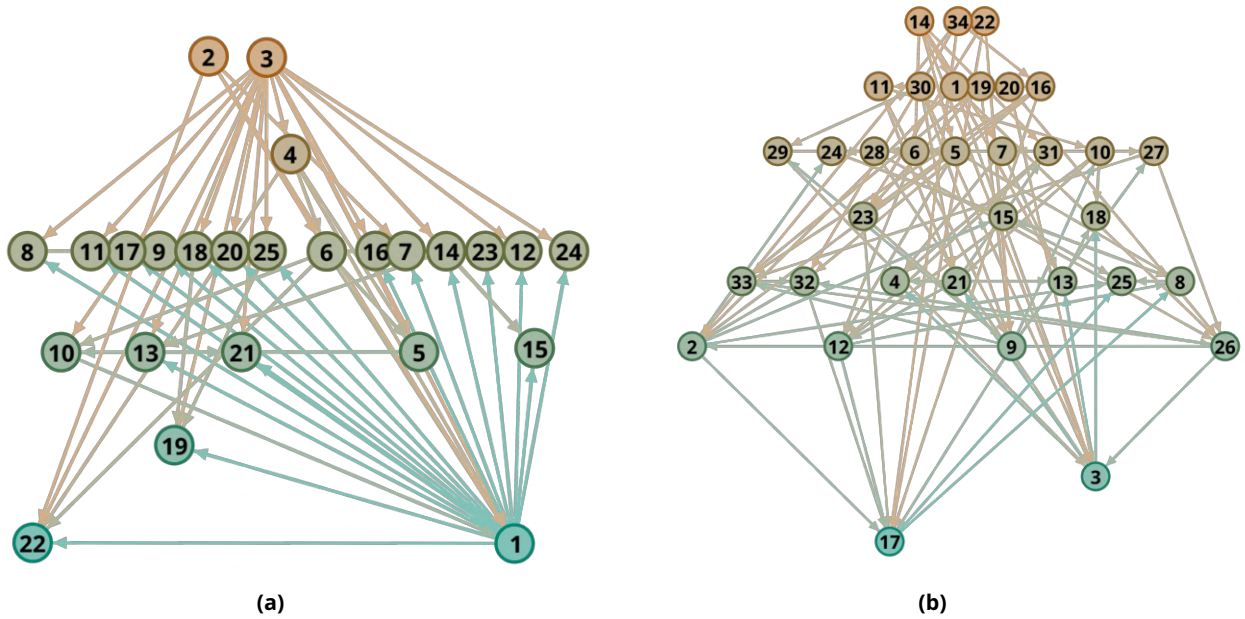


**Figure 9.** Hierarchical graph diagram based on indegree created with Gephi (Bastian et al., 2009) (node color = indegree (brown: low, turquoise: high), link color = indegree of source node, y-position: indegree); (a) GdF 207; (b) GdF RF.c\_49

stand the OS becomes a cognitive challenge. GdF 207 is a blade, and has therefore been knapped from the surface of a core, and as a result shows only partly the negatives and hence the complexity of the OS before. 299 300

To change perspective and focus on a core, GdF RF.c\_49 is analyzed (Fig 9 (b), Fig 10). In addition, this artifact already had an OS in the form of a drawing (Falcucci, Conard, et al. (2017)). The possible applications of the scar and ridge properties of adjacency graphs are numerous, from simple statistical parameters that can be assigned to either the scars or the ridges, such as the mean, median, and standard deviation of a parameter, e.g., the surface area, to parameters derived directly or indirectly from the relationship between scars and ridges. 301 302 303 304 305 306

To obtain the direction of a connection and to evaluate this interpretation, this research uses the relative difference in area, degree, and betweenness of two adjacent scars. To calculate the area of the scars, sub-meshes of the labels were created and their surface area was calculated. 307 308 309 310 311

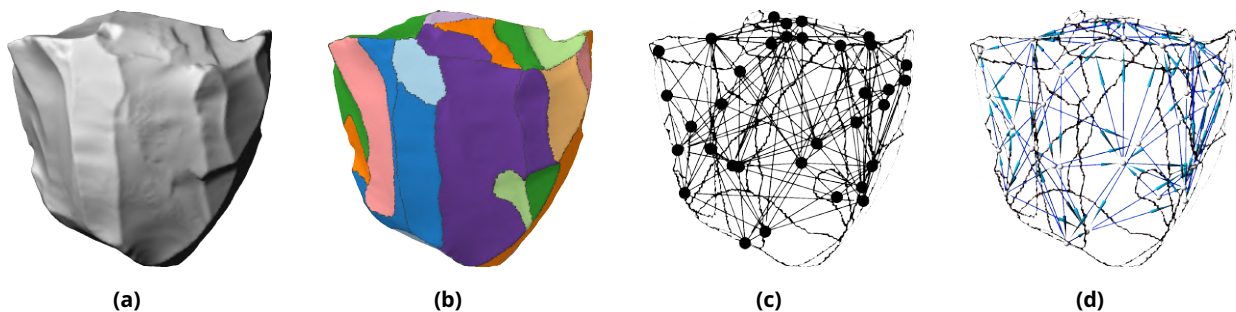


**Figure 10.** (a) 3D mesh of *GdF RF.c\_49*; (b) ground truth label; (c) adjacency graph model; (d) graph model (direction = Falcucci, Conard, et al., 2017)

## Parameter Directed Graphs and Evaluation

312

The accuracy of GdF 207 and GdF RF.c\_49 differ and represent the range of accuracy of the graph computation. While the accuracy of GdF 207 ranges from 78 to 84 %, the accuracy of GdF RF.c\_49 ranges from 49 to 53% (Tab. 1). The difference can be partly explained by their object categories: while GdF 207 is a retouched blade from which several small flakes have been removed along the edges, leading to a strong connection between dorsal and ventral scars along the edges without regard to their position in the OS, GdF RF.c\_49 is a core from which flakes of more similar size have been removed. Due to the completely different ways in which Paleolithic people handled these artifacts, one as a source for tools and the other as a tool itself, the scar patterns naturally differ.

313

314

315

316

317

318

319

320

321

Accuracy of the graph models		
	Artifacts	
Parameter	GdF 207	GdF RF.c_49
Area	84%	52%
Degree	78%	49%
Betweenness	79%	53%

**Table 1.** Evaluation Link Directions of Graph Models according to Area, Degree and Betweenness

In both cases, the relative area, degree and betweenness of the scars lead to similar results, with only a range of 6 % (GdF 207) and 4 % (GdF RF.c\_49). This could possibly be explained by an underlying relationship between the size of a scar and its relevance in the graph. Fig 11 shows that GdF 207 contains prominent outliers that have an impact on all parameters considered.

322

323

324

325

326

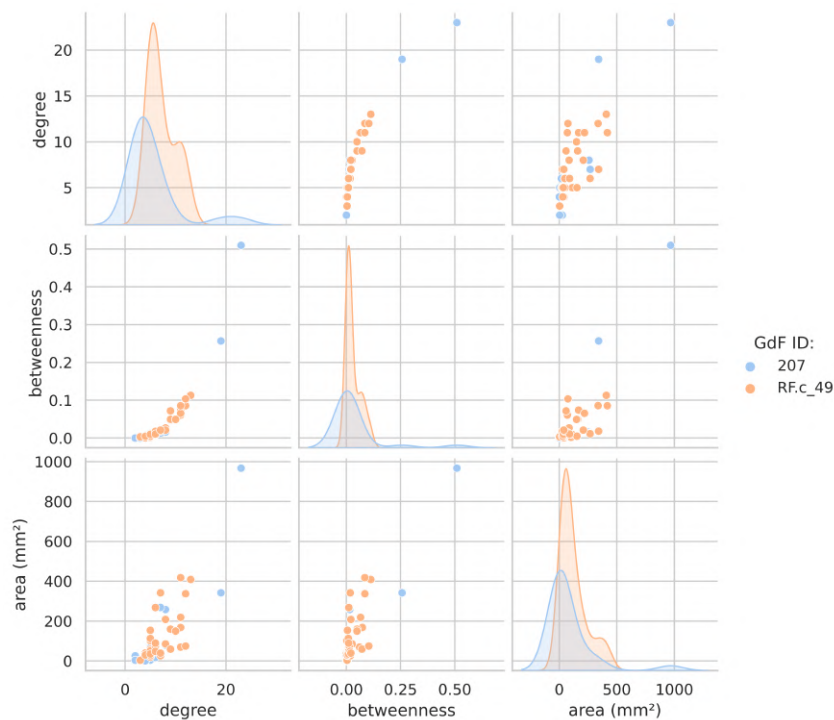


**Figure 11.** Comparison of area (mm<sup>2</sup>), degree and betweenness of the scars of GdF RF.c\_49 and GdF 207

Even without considering the poor results of GdF RF.c\_49, the graph models for GdF 207 have difficulties detecting the correct relationship between dorsal scars, which are either similar in size or earlier scars have been overwritten by later ones. Furthermore, dorsal-ventral links are also prone to error, as the most prominent ventral scar is the largest scar on the artifact, considering that it is almost complete. This scar is the youngest scar on the artifact, not considering later retouches. But it is one of the earliest, according to all the data derived from the graph models.

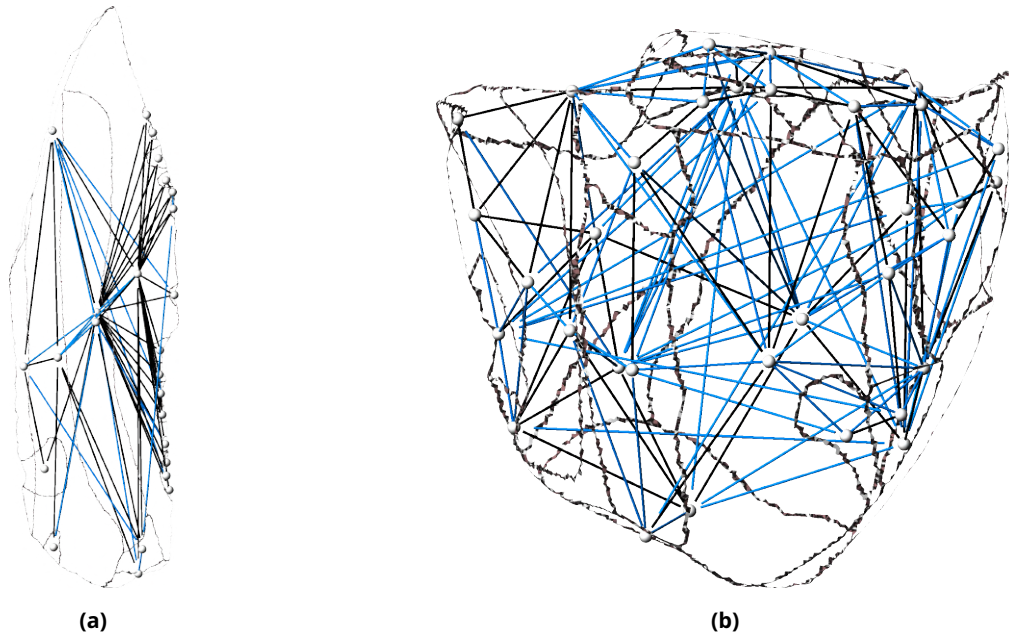


**Figure 12.** Evaluation of best performing directions (black = true; blue = false); (a) GdF 207: Area ("greater"); (b) GdF RF.c\_49: Betweenness ("lower")

As using graph models have been successfully used to describe complex situations allowing for queries and visualizations, it will help to understand the underlying patterns. A similar effect can be expected for the question of determining OS's. Having a small number of easily understandable parameters is by design to make the approach accessible for a wider range of users. Automatic determination of parameters will be a next step. Furthermore the graph representation can also be useful for teaching OS's conceptually.

## Outlook and further Applications

One of the central challenges in archaeology is the lack of open, digitized data that can be used to evaluate automated approaches, which applies in particular to 3D models, segmentations and OS's. This limits the development of new methods and ultimately restricts the scope of future research. To address this, we have published along this article our annotated dataset (Linsel et al., 2023), which we used to evaluate our segmentation algorithm (Bullenkamp et al., 2023). The OS's are still subject to ongoing research and will be published later. However, we are expanding our dataset to include more manually annotated artifacts by scanning lithic artifacts, e.g., leaf points from different sites, creating graph models, and adding OS's as well.

One of the key limitations of exclusively examining artifacts in the absence of their position within an OS is the dependency on surface properties and expert knowledge. To ensure the accuracy of a 3D OS dataset, we will aim to incorporate 3D data from experimental knapping series where the connection between positive and negative scars within an OS is documented in future work. Merging a complete OS Graph with 3D data will lead to the development of a more precise GT dataset, enabling us to adapt methods to real datasets.



## Relative Chronology of Scars (OS)

352

We are currently working on new methods to determine OS's automatically. As discussed in this article, the results of the graph model-based OS are promising but due the univariate method, and the small dataset used to determine the direction, the results and the gained insights are limited. Hence, one of the next needed steps is to combine multiple parameters of more artifacts in the graph model to obtain a better insight of the internal mechanics of the knapping process and as a result of the OS's. In this regard, we are currently working on implementing two methods, which are derived from the archaeological practice described by Pastoors et al. (2015).

353

354

355

356

357

358

359

360

This research serves as a first step towards abstracting human lithic tools in a simplified and computer-readable way. We do consider our graph models of individual tools as intermediate result being a data source for graph-based machine learning, which has shown great potential in recognizing cuneiform signs (Kriege et al., 2018), and ultimately as a stepping stone towards a more detailed understanding of lithic technologies.

361

362

363

364

## Acknowledgements

365

We thank Jürgen Richter for his help in creating the OS's. We also thank Ernst Max Stötzner for his contributions to GigaMesh and Rebecca Gnau for her help in creating the validation data for the graph models. We thank Sebastian Hageneuer for his role as PCI recommender and to the two reviewers for sharing their valuable suggestions.

366

367

368

369

## Fundings

370

This research was directly funded by the Martin-Luther University Halle-Wittenberg and conducted at the Institute of Computer Science.

371

372

## Conflict of interest disclosure

373

The authors declare that they comply with the PCI rule of having no financial conflicts of interest in relation to the content of the article.

374

375

## Data, Script, Code and Supplementary Information Availability

376

In addition to this publication, we provide a code publication of the segmentation (Bullenkamp et al., 2023) and a data publication (Linsel et al., 2023). Due to the early stage of the graph models, which were heavily inspired by the discussion at the CAA conference, we cannot provide its code and data at this stage of our research.

377

378

379

380

## References

- Barone S, A Paoli, P Neri, A Razionale, MD Santis, and F Mailland (June 2018). Automatic illustration of lithics from 3d scanned models. *IOP Conference Series: Materials Science and Engineering* 364, 012017. <https://doi.org/10.1088/1757-899X/364/1/012017>.
- Bastian M, S Heymann, and M Jacomy (2009). Gephi: an open source software for exploring and manipulating networks. In: *Third international AAAI conference on weblogs and social media*.
- Bullenkamp JP, T Häberle, and H Mara (Aug. 2023). *MorseMesh*. Version v0.1. <https://doi.org/10.5281/zenodo.8297368>.
- Cignoni P, M Callieri, M Corsini, M Dellepiane, F Ganovelli, and G Ranzuglia (2008). MeshLab: an Open-Source Mesh Processing Tool. In: *Eurographics Italian Chapter Conference*, pp. 129–136. <https://doi.org/10.2312/LocalChapterEvents/ItalChap/ItalianChapConf2008/129-136>.
- Falcucci A, NJ Conard, and M Peresani (Dec. 2017). A critical assessment of the Protoaurignacian lithic technology at Fumane Cave and its implications for the definition of the earliest Aurignacian. *PLOS ONE* 12, 1–43. <https://doi.org/10.1371/journal.pone.0189241>.
- Falcucci A and M Peresani (2022a). *The Open Aurignacian Project. Volume 1: Fumane Cave in northeastern Italy*. Version 2.1.1. Zenodo. <https://doi.org/10.5281/zenodo.7664308>.
- Falcucci A and M Peresani (2022b). *The Open Aurignacian Project. Volume 1: Fumane Cave in northeastern Italy*. Version 1.0.0. Zenodo. <https://doi.org/10.5281/zenodo.6362150>.
- Forman R (2001). A User's Guide To Discrete Morse Theory. *Séminaire Lotharingien de Combinatoire* 48, B48c–35.
- Gellis JJ, CR Smith, and RA Foley (2022). PyLithics: A Python package for stone tool analysis. *Journal of Open Source Software* 7, 3738. <https://doi.org/10.21105/joss.03738>.
- Herzlinger G and L Grosman (2018). AGMT3-D: A software for 3-D landmarks-based geometric morphometric shape analysis of archaeological artifacts. *PLOS ONE* 13, 1–17. <https://doi.org/10.1371/journal.pone.0207890>.
- Higham T, F Brock, M Peresani, A Broglio, R Wood, and K Douka (2009). Problems with radiocarbon dating the Middle to Upper Palaeolithic transition in Italy. *Quaternary Science Reviews* 28, 1257–1267. <https://doi.org/10.1016/j.quascirev.2008.12.018>.
- Homburg T, R Zwick, H Mara, and KC Bruhn (May 2022). Annotated 3D-Models of Cuneiform Tablets. *Journal of Open Archaeology Data* 10. <https://doi.org/10.5334/joad.92>.
- Kriege NM, M Fey, D Fisseler, P Mutzel, and F Weichert (2018). Recognizing Cuneiform Signs Using Graph Based Methods. <https://doi.org/10.48550/arXiv.1802.05908>. arXiv: 1802.05908 [cs . CV].
- Linsel F, JP Bullenkamp, and H Mara (2023). *3D Data Derivatives of Grotta di Fumane: GigaMesh-processed, Annotations and Segmentations*. Version 1.0.0. Zenodo. <https://doi.org/10.5281/zenodo.8288967>.
- Maier A, R John, F Linsel, G Roth, W Antl-Weiser, L Bauer, N Buchinger, L Cavak, H Hoffmann, J Puschmann, M Schemmel, VC Schmid, U Simon, and R Thomas (May 2023). Analyzing Trends in Material Culture Evolution—a Case Study of Gravettian Points from Lower Austria and Moravia. *Journal of Paleolithic Archaeology* 6, 15. ISSN: 2520-8217. <https://doi.org/10.1007/s41982-023-00145-z>.
- Mara H and S Krömker (2013). Vectorization of 3D-Characters by Integral Invariant Filtering of High-Resolution Triangular Meshes. In: *2013 12th International Conference on Document Analysis and Recognition*, pp. 62–66. <https://doi.org/10.1109/ICDAR.2013.21>.
- Mara H, S Krömker, S Jakob, and B Breuckmann (2010). GigaMesh and Gilgamesh 3D Multiscale Integral Invariant Cuneiform Character Extraction. In: *VAST: International Symposium on Virtual Reality, Archaeology and Intelligent Cultural Heritage*. Ed. by Artusi A, Joly M, Lucet G, Pitzalis D, and Ribes A. The Eurographics Association. ISBN: 978-3-905674-29-3. <https://doi.org/10.2312/VAST/VAST10/131-138>.

- Marín-Arroyo AB, G Terlato, M Vidal-Cordasco, and M Peresani (2023). Subsistence of early anatomically modern humans in Europe as evidenced in the Protoaurignacian occupations of Fumane Cave, Italy. *Scientific Reports* 13, 3788. <https://doi.org/10.1038/s41598-023-30059-3>. 426  
427  
428
- Pastors A (2000). Standardization and Individuality in the Production Process of Bifacial Tools - Leaf-shaped Scrapers from the Middle Paleolithic Open Air Site Saré Kaya I (Crimea). A contribution to understanding the method of Working Stage Analysis. In: *Neanderthals and Modern Humans - Discussing the Transition. Central and Eastern Europe from 50.000 - 30.000 B.P.* Neanderthal Museum, pp. 243–255. 429  
430  
431  
432
- Pastors A, Y Tafelmaier, and GC Weniger (2015). Quantification of late Pleistocene core configurations: Application of the Working Stage Analysis as estimation method for technological behavioural efficiency. *Quartär* 62, 62–84. [https://doi.org/10.7485/QU62\\_3](https://doi.org/10.7485/QU62_3). 433  
434  
435
- Pop CM (Apr. 2019). *cornelmpop/Lithics3D: v0.4.2*. Version v0.4.2. <https://doi.org/10.5281/zenodo.2648097>. 436
- Pulla S, A Razdan, and G Farin (2001). Improved curvature estimation for watershed segmentation of 3-dimensional meshes. *IEEE Transactions on Visualization and Computer Graphics* 5, 308–321. 437  
438
- Richardson E, L Grosman, U Smilansky, and M Werman (2014). Extracting Scar and Ridge Features from 3D-scanned Lithic Artifacts. *Archaeology in the Digital Era: 40th Annual Conference of Computer Applications and Quantitative Methods in Archaeology (CAA)*, 83–92. <https://doi.org/10.1515/9789048519590-010>. 439  
440  
441
- Richter J (1997). Sesselfelsgrotte III. *Der G-Schichten-Komplex der Sesselfelsgrotte. Zum Verständnis des Micoquien. Quartär-Bibliothek* 7. 442  
443
- Richter J (2004). Copies of flakes: operational sequences of foliate pieces from Buran-Kaya III level B1. *The Middle Paleolithic and Early Upper Paleolithic of Eastern Crimea* 3, 233–247. 444  
445
- Robins V, P Wood, and A Sheppard (2011). Theory and Algorithms for Constructing Discrete Morse Complexes from Grayscale Digital Images. *IEEE transactions on pattern analysis and machine intelligence* 33, 1646–1658. <https://doi.org/10.1109/TPAMI.2011.95>. 446  
447  
448
- Shea JJ (2013). Lithics Basics. In: *Stone Tools in the Paleolithic and Neolithic Near East: A Guide*. Cambridge University Press, pp. 17–46. <https://doi.org/10.1017/CBO9781139026314.003>. 449  
450
- Weiss M (Oct. 2020). The Lichtenberg Keilmesser - it's all about the angle. *PLOS ONE* 15, 1–31. <https://doi.org/10.1371/journal.pone.0239718>. 451  
452
- Yang X, K Matsuyama, and K Konno (2017). Interactive visualization of assembly instruction for stone tools restoration. In: *2017 IEEE Pacific Visualization Symposium (PacificVis)*, pp. 270–274. <https://doi.org/10.1109/PACIFICVIS.2017.8031604>. 453  
454  
455